Effects of Hatch Distance and Spray Pattern on Film Morphology in Micro-Cold Spray

Ronnie F. P. Stone*, Arun Ruhfus*, Minh Le*, Emmanuel Ekoi*, Desiderio Kovar*, Zhenghui Sha* [1]

* Center for Additive Manufacturing and Design Innovation, Walker Department of Mechanical Engineering, The University of Texas at Austin, TX 78712

Abstract

Micro-Cold Spray (MCS), also known as the Aerosol Deposition Method (ADM), is a solid-state that enables the formation of dense, thick films at room temperature. One challenge is that precise geometric control remains difficult due to complex deposition dynamics, similar to cold spray and thermal spraying. This limitation hinders the advancement of MCS as a direct-write additive manufacturing (AM) method, particularly for micro-electromechanical systems applications. A critical yet underexplored factor in achieving geometric control is the spray path. While preliminarily studied in traditional cold spray, a systematic investigation in MCS is lacking. This paper presents the first experimentally validated study of how hatch distance and spray pattern, specifically normal and overlapping serpentine paths, affect MCS film morphology. By analyzing film adhesion and surface roughness, we offer new insights into deposition control, advancing the potential of MCS as a viable AM technology.

Keywords: Additive Manufacturing, Micro-Cold Spray, Film Surface Morphology.

1. Introduction

Micro-cold spray (MCS) is an emerging solid-state spraying technology with promising applications in the deposition of metal and ceramics films [1, 2, 3]. Unlike traditional cold spray [4], MCS uses lower absolute pressures and smaller powder particles (e.g., $<2\mu m$). It also does not require pre-heating the carrier gas used to aerosolize the feedstock. As such, it is able to deposit thick films on temperature-sensitive substrates to near full-density [3]. While researchers have made significant advances in understanding the underlying physics of MCS in terms of, for example, critical impact velocities [5], agglomerate morphology [6], and even composite films [7], the surface morphology of deposited films remains comparatively underexplored in the existing literature.

The surface morphology of MCS films is critical for several reasons. Traditionally, it has been examined to assess film density, typically inferred from the absence of large pores, and to analyze microstructural features at the nanoscale. The resulting high-density, gas-tight surfaces, often comparable to the bulk material, are essential for various material applications in film and coating deposition [8, 9]. In our work, however, we aim to leverage MCS as a true additive manufacturing (AM) process, where the primary surface morphology characteristic of interest is layer flatness (Section 3). Similar to traditional cold spray (CS), building up material layer by layer in MCS remains a significant challenge due to the inherent physics of the process, often leading to gradual reductions in the deposition rate with film thickness [10, 11, 12]. Since the ability to fabricate 3D features is fundamental to AM, achieving a controllable and consistent surface morphology is a key requirement. For MCS to advance beyond thin film deposition and to allow it to produce

[1] Corresponding author: zsha@austin.utexas.edu

microscale devices, similar to other advanced spraying processes [13], it must enable high-quality, repeatable deposition across multiple layers.

As such, in this study, we investigate the effects of hatch spacing and spray pattern on surface roughness and film adhesion in MCS. Hatch spacing refers to the distance between adjacent passes of the spray nozzle, while spray pattern describes the trajectory or motion strategy used by the nozzle during deposition (e.g., serpentine or overlapping paths; see Section 2 for details). By systematically varying these parameters and characterizing the resulting quality metrics, we aim to identify process conditions that promote smoother surfaces and stronger adhesion between layers. These two parameters were chosen not only because they directly influence deposition quality, but also because they are among the few variables that remain highly configurable during the printing process. While many aspects of the MCS setup, such as gas type, chamber pressure, or powder morphology, are often fixed by hardware or experimental constraints, the motion strategy of the dynamic stage remains under user control. As a result, hatch spacing and spray pattern present accessible, tunable levers for improving part quality. The ultimate goal of this study is to develop practical insights and guidelines for process planning in layer-wise MCS, enabling more reliable multi-layer fabrication and advancing the transition of MCS from a coating method to a fully functional micro-scale AM technique.

The remainder of the paper is organized as follows. Section 2 describes the conceptual framework, based on which we motivate our exploration. In Section 3, we provide an overview of the experimental setup and the design of experiments methodology. Finally, in Section 4 we discuss the results more broadly and stress future research directions.

2. Conceptual Framework

Fundamentally, we want to understand whether, and to what extent, hatch spacing and spraying pattern choices can affect the surface morphology of MCS films. In particular, we are interested in assessing how these parameters can be tuned to produce good films, that is, with desired surface roughness metrics values (e.g., areal arithmetic mean height S_a). As we want to leverage MCS as a true additive manufacturing technology, it is important that the film is generally flat throughout the deposition process so the Z-directional features can be achieved layer by layer. There are two key reasons for this requirement. First, it is a well-known fact that particles need to reach a critical velocity (v_c) when impacting the substrate to successfully adhere to it. However, if the surface is not perpendicular to the spray cone, the component of the kinetic energy in the direction needed for deposition is reduced, and the particles may end up bouncing off of the film. Therefore, high film roughness can directly impact the deposition efficiency and the ability of the film to build up properly. Second, the creation of 3D features in additive manufacturing demands that each layer adheres to strict spatial tolerances. If a given layer is poorly deposited, exhibiting significant deviations in thickness or geometry, it can compromise the quality of all subsequent layers, ultimately leading to failure of the entire build (Fig. 1). Therefore, it is essential that MCS films provide a sufficiently uniform and stable foundation for continued deposition, much like how FDM-printed layers must maintain printability to support subsequent extrusion.

It is important to recognize that hatch spacing and spray pattern are not the only process parameters that significantly influence the surface morphology of MCS films. Like other additive manufacturing methods, MCS depends on various parameters that collectively influence final part

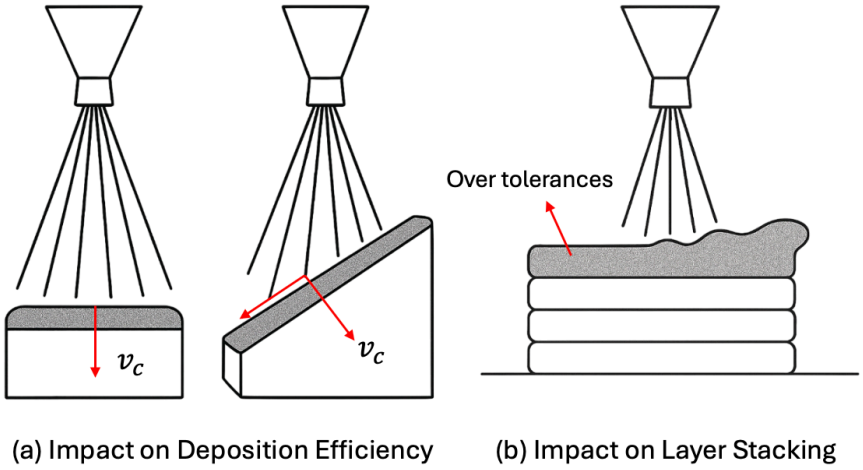

Figure 1: Key impacts of surface roughness on MCS manufacturing quality.

quality. For instance, factors such as the agglomerate morphology and standoff distance (SoD) have been shown to strongly affect surface roughness, measured by arithmetic mean roughness R_a and root mean square (RMS) roughness R_q [14, 15, 16]. However, many of these parameters including choice of inert gas, and chamber pressure, are typically fixed by experimental setup or constrained by equipment limitations, leaving little room for adjustment. In contrast, users often retain substantial flexibility in how the dynamic stage moves during deposition. For this reason, we focus our study on hatch spacing and spray pattern, as they offer practical opportunities for tuning and may be of direct value to researchers.

As detailed in Section 3, our design of experiments (DOE) focuses on two primary spray pattern choices: serpentine and overlapping. Serpentine patterns, also known as zig-zag or raster patterns, are traditionally used in additive manufacturing, particularly in FDM. We include them in our study because they represent a conventional approach that many users are likely to adopt. In contrast, overlapping patterns are less commonly used but are included due to our interest in multi-nozzle MCS systems [17]. In this context, we envision a smaller-throat-diameter nozzle being used to spray between previously deposited lines created by a larger-diameter nozzle. The motivation is that the smaller nozzle could fill in or flatten regions of the film that were underfilled or where powder failed to adhere properly (Fig. 2).

Our selection of hatch spacing is also partially guided by this multi-nozzle context. Assuming the deposition profile from a single pass follows a pseudo-Gaussian distribution, which has been observed in the literature [6, 18], and that the powder adheres well, then we can analytically determine the ideal (i.e., in terms of theoretical flatness) hatch spacing for overlap with a smaller nozzle in Eq. (1):

$$\epsilon = \left(\frac{A_2}{A_1} + 1\right) \sigma_1 \sqrt{2\pi}, \tag{1}$$

where σ_1 is the standard deviation of the Gaussian profile representing the cross-sectional profile

of the line deposition with the larger nozzle, and A_1 and A_2 are the cross-sectional areas of the deposition for the larger and smaller nozzles, respectively. However, since we are currently only using one nozzle for these experiments, we have $A_1 = A_2$ and Eq. (1) reduces to $\epsilon = 2\sigma\sqrt{2\pi}$. This value, derived from the standard deviation σ of the Gaussian profile, serves as the center point in our DOE. To define the upper bound of the hatch spacing range, we use 6σ, beyond which neighboring lines have negligible overlap. To preserve symmetry around the center point in the DOE, we define the lower bound by subtracting the same offset $\delta\epsilon = (6 - 2\sqrt{2\pi})\sigma$ used to reach the upper bound, ensuring a balanced exploration of parameter space.

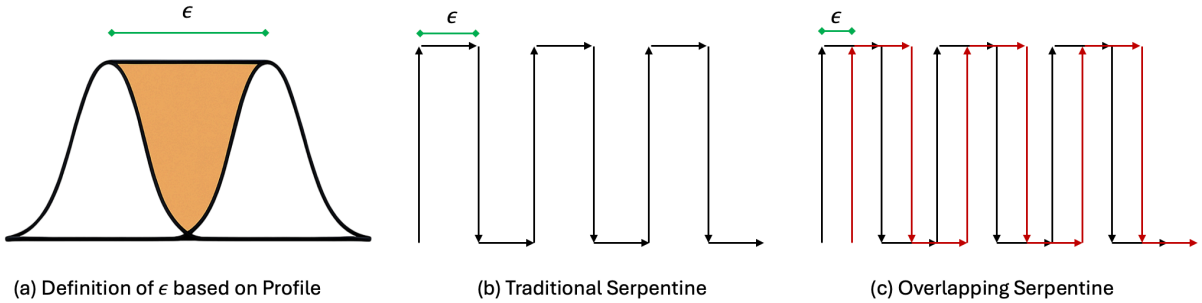

Figure 2: Summary of how the hatch spacing range and spraying patterns were determined.

3. Methodology

3.1. Physical System Description

The MCS machine used in the experiments consists of three main systems: the gas, the vacuum, and the gantry systems (Fig. 3). The gas and the vacuum systems are controlled via the AutomationDirect P1-550 PLC board along with its I/O modules, while the gantry system is controlled by a Duet 6XD board due to its ability to easily interpret and precisely follow G-code, needed for the fine-tuning of spraying patterns utilized in the experiments.

Generally, the vacuum system consists of a roughing pump and a Roots booster assembly which drop the process chamber to approximately 1 Torr. The gas system, which connects the carrier gas cylinder to the deagglomerator and the nozzle, is responsible for aerosolizing the particles. The resulting aerosol is then flown through a feeder system, and is accelerated through the nozzle to the desired critical velocity. Finally, the gantry is responsible for moving the substrate in all three degrees of freedom, and is wired to a Duet board, which runs RepRap firmware for controlling the overlap and serpentine patterns mentioned in the conceptual framework (Section 2). As for general process parameters, which are held constant throughout the deposition, we provide a table summarizing them in Table 1.

3.2. Design of Experiments

Our DOE consists of two process parameters (i.e., the control variables), that are spray pattern and hatch spacing, and two response variables, that are adhesion and film roughness. For the experiment, a number of parameters were kept constant (Section 5.1). Adhesion is observed qualitatively by observing whether the film adheres appropriately to the substrate after deposition and then again after cleaning. Roughness can be assessed both in its two-dimensional metric of areal arithmetic mean height (S_a) by looking at the entire film surface, or its one-dimensional counterpart (R_a), by

looking at specific lines of interest in the film (Fig. 4). We have also considered total waviness (W_t) due to the scale of the film thickness with respect to the agglomerate morphology [19] (see Section 5).

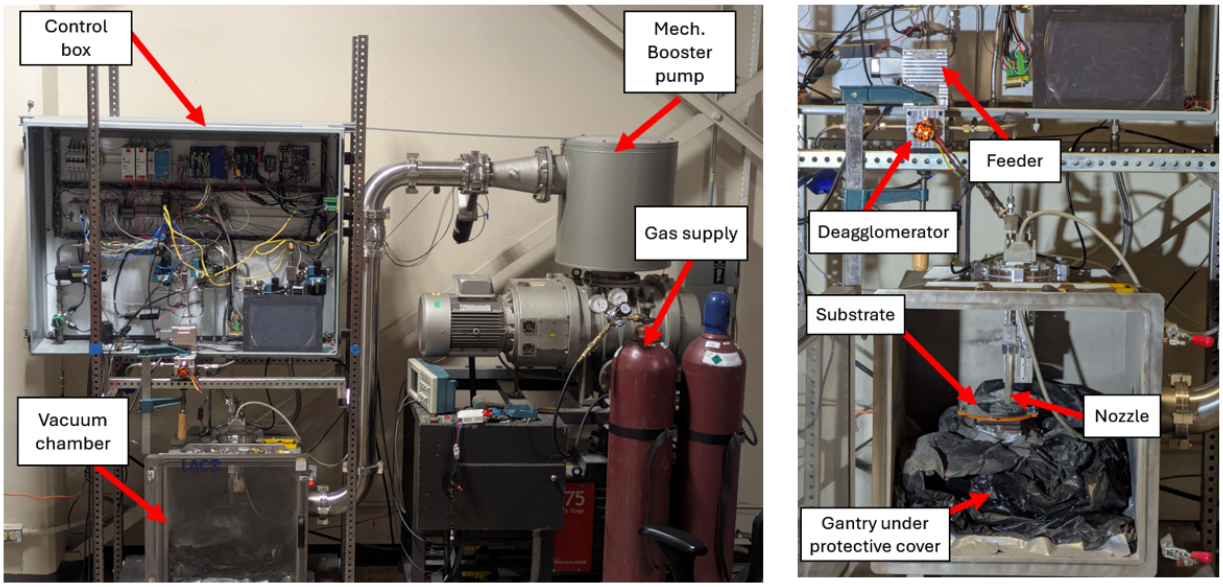

Figure 3: Overview of the MCS system used in the experiments.

Table 1: Summary of Process Parameters

Parameter	Value	Units
Nozzle Type	De Laval	-
Nozzle Throat Diameter	1	mm
Standoff Distance	12	mm
Scan Speed	10	mm/s
Powder Feeder Frequency	200	RPM
Deagglomerator Flow Rate	6	slpm
Bypass Flow Rate	8	slpm
Deagglomerator Pressure	799	Torr
Bypass Pressure	761	Torr
Chamber Pressure	1	Torr
Inert Gas Type	Helium	-
Inert Gas Purity	4.8	-
Substrate Material	Silicon	-
Powder Material	Silver	-
Average Particle Size	200-300	nm

All the silicon wafer substrates, with a diameter of 150 mm, were subjected to a standardized cleaning process prior to deposition. Each wafer was first rinsed with a soapy solution, prepared

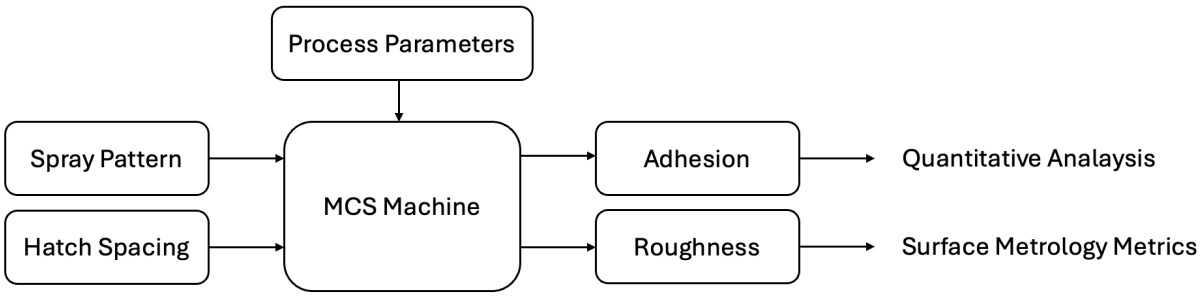

Figure 4: Outline of the DOE, highlighting control, response variables, and process parameters.

by diluting one-part solution with two parts water, and then dried using compressed air. This was followed by rinses with acetone and isopropanol (IPA), again using compressed air drying after each step to ensure the removal of any solvents or contaminants.

The use of silicon wafers as substrates was motivated by two primary factors. First, their hard, flat surface presents one of the most challenging conditions for adhesion, making them a recognized worst-case scenario for deposition. Demonstrating successful deposition on wafers therefore implies feasibility on softer or rougher surfaces. Second, silicon wafers are ubiquitous in the semiconductor industry, making them directly relevant for device fabrication and highlighting their suitability for exploring micro-cold spray (MCS) as an additive manufacturing technology.

To experimentally determine the ϵ parameter in Eq. (1), two initial runs were carried out to determine the width of the deposited line and calibrate the Gaussian profile. The two runs consisting of two serpentine patterns, each containing four lines, and a pitch of 10 mm ensures the complete separation of lines for accurate measurement. The only difference between the two runs was the number of passes, which were 20 and 40, respectively. The resulting depositions were examined using a Keyence VHX 7100 digital microscope (Fig. 6a), and by comparing the adhesion quality of the two runs, we decided to focus on specimen made with 40 passes, since it produced depositions with better adhesion quality. Width measurements from 8 lines were taken (Fig. 5), and the value of σ used was based on their average as shown in Table 2.

Table 2: Measured Line Widths of 40 Passes Specimen

Line Number	Measured Width (mm)
1	4.17
2	4.02
3	4.04
4	4.06
5	4.89
6	4.88
7	4.83
8	4.86
Average	**4.47**

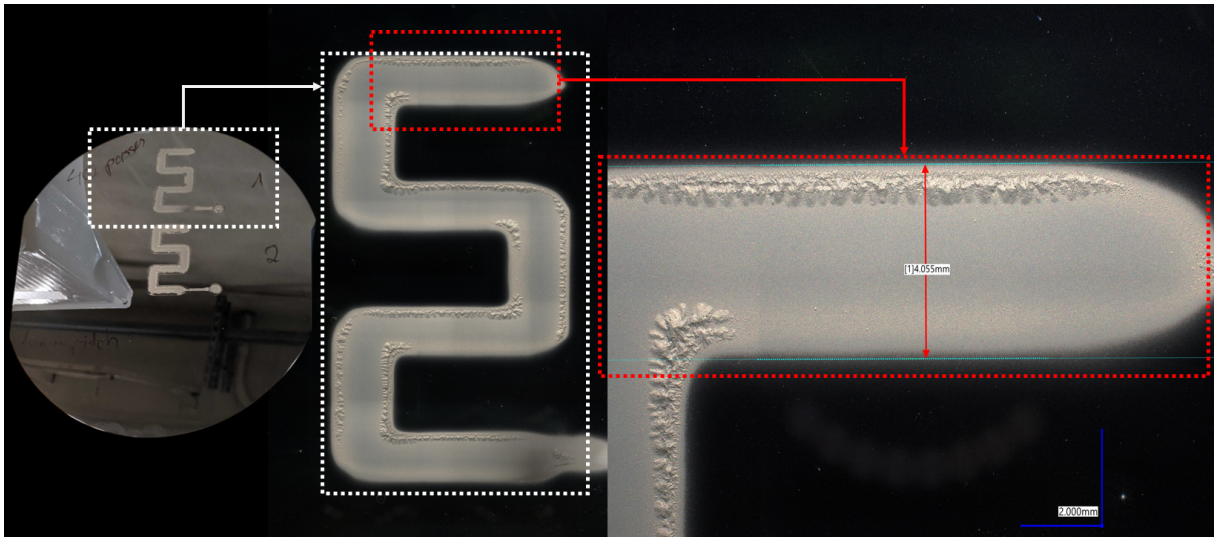

Figure 5: Determining profile width with 40-passes specimen. One of the eight measurement used is highlighted here.

During the depositions, silicon wafers were positioned using a standoff distance of 10 mm, and carefully aligned to ensure sufficient space for three passes along the Y-axis. The deagglomerator and feeder were activated and allowed to reach steady-state prior to starting the sample patterns. The feedstock chosen for this experiment is ultrafine silver powder from Solvus.

Our DOE followed a full factorial design. Thus, for each wafer, three samples were deposited, and grouped according to the spraying pattern and hatch spacing. Each wafer was sprayed with hatch spacings of ϵ (middle spacing), $\epsilon - \delta\epsilon$ (lower spacing) and $\epsilon + \delta\epsilon$ (upper spacing) for either the traditional or overlapping serpentine pattern. This grouping is summarized in Table 3. Upon completion of each pattern set, the wafer was replaced and the process repeated for the next set of conditions.

Table 3: Experiment Runs Based on Full Factorial DOE

Wafer	Hatch Spacing	Spraying Pattern
a	ϵ	Regular Serpentine
a	$\epsilon - \delta\epsilon$	Regular Serpentine
a	$\epsilon + \delta\epsilon$	Regular Serpentine
b	ϵ	Overlapping Serpentine
b	$\epsilon - \delta\epsilon$	Overlapping Serpentine
b	$\epsilon + \delta\epsilon$	Overlapping Serpentine

After deposition, all samples were taken and examined using the digital microscope (Fig. 6a). For each pattern, a 3D image was constructed by stitching together 50 vertically spaced images taken at 100$\times$ magnification, covering the full height range of the deposited material. A linear profile was then extracted across the length of each pattern, averaging eight lines spaced 400 μm apart and centered on the pattern to avoid edge effects at the ends of each serpentine. Surface

roughness measurements were performed over a 12 mm wide region, spanning from the center of the two outermost path lines, as illustrated in Figure 6b. All measurements were initially conducted on as-deposited samples, with the analysis repeated after a post-deposition cleaning step.

The post-deposition cleaning procedure involved gently wiping each sample with a folded laboratory tissue wipe, followed by a second wipe using tissue wipe soaked in IPA. Finally, the samples were dried using compressed air to ensure the removal of any residual particles or cleaning agents. As mentioned, adhesion was measured qualitatively at this step, observing how the film adhered to the substrate after cleaning. A flowchart is also provided summarizing the methodology, starting from substrate preparation, all throughout the surface metrology process (Fig. 7).

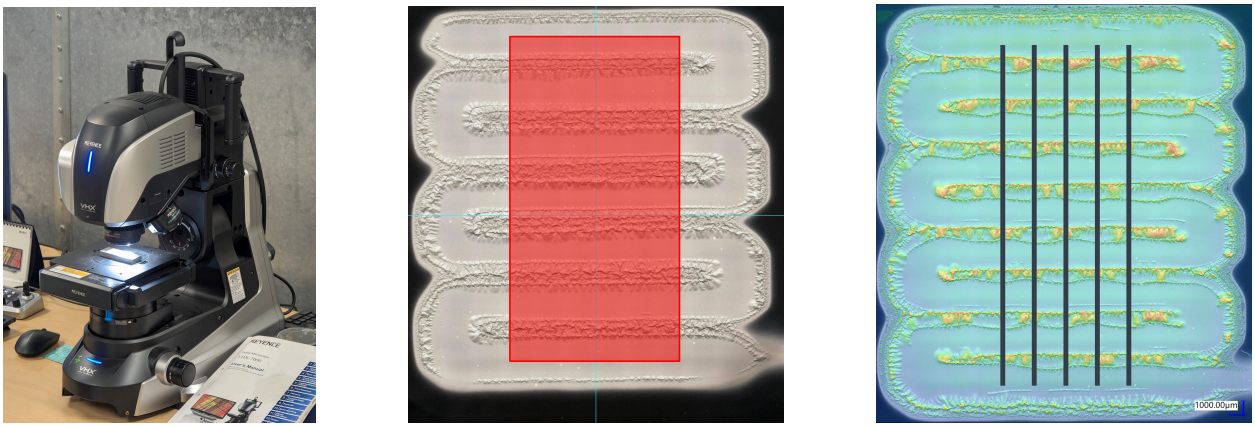

(a) A Keyence VHX 7100 digital microscope.

(b) Surface roughness capture area to avoid edge effects.

(c) Example of how perpendicular line profiles were captured.

Figure 6: Digital microscope information and data capture workflow.

5. Results

To validate our proposed methodology and to better understand how hatch distance and spray pattern affect film morphology in MCS, we carried out a series of physical studies as laid out by our design of experiments. All experiments were conducted using the same MCS machine, keeping all other process parameters nominally constant throughout the depositions.

Initial visual inspection revealed distinct morphological differences across the deposited samples. As can be seen in Figure 8b, areas directly under the nozzle path exhibited relatively flat surfaces, while adjacent regions displayed significantly rougher morphologies. The deposition process had variability in quality, with clear distinctions between good and bad passes as evidenced by the perpendicular profile measurements as can be seen in Figure 8a. Good profiles were characterized by consistent flat sections at regular heights, indicating uniform material deposition. In contrast, bad profiles exhibited extreme height variations, with inconsistent surface features, most likely due to delamination from the substrate (see Section 6). The rough areas next to the nozzle path served as the initiation points for delamination, suggesting a relationship between surface morphology and adhesion failure.

Analysis after cleaning revealed that serpentine spray patterns demonstrated superior adhesion compared to the overlap spray pattern. The middle spacing showed the best overall adhesion per-

formance. Conversely, overlap patterns exhibited more severe defects, with material flaking of the substrate during deposition and the entire deposition detaching during the cleaning process (see Appendix for direct comparisons).

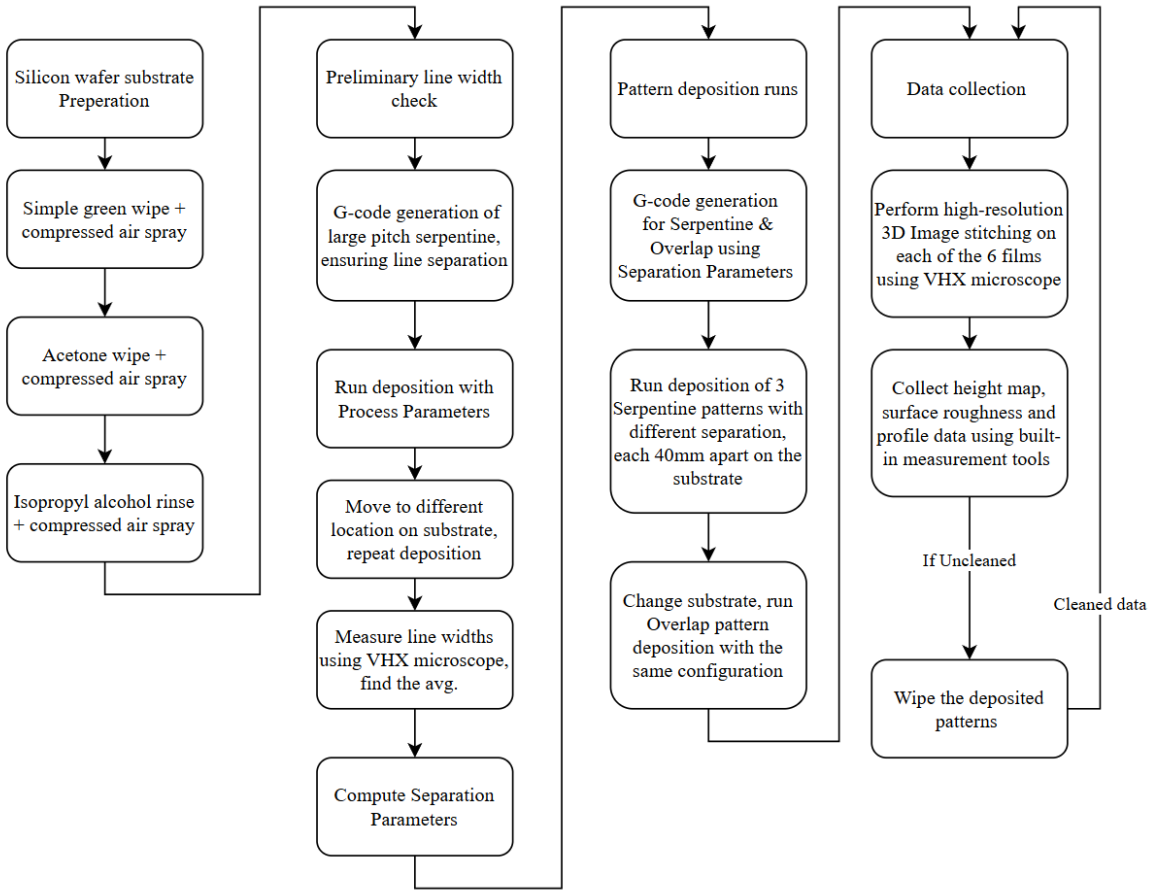

Figure 7: Flowchart summarizing the experimental methodology.

The results of the line roughness (R_a) analysis using parallel profiles is presented in Figure 9. The cutoff parameters λ_s = none and λ_c = 800 μm where used for calculating the values. In the figure, the solid colors represent the as-deposited results while the striped pattern represent the data from samples after cleaning. The as-deposited samples had some variance in results, and except for the serpentine upper spacing condition, samples 2 and 3 tend to have very similar roughness, while sample 1 was an outlier with roughness values in line with the cleaned results for most depositions. Then after cleaning the measurements become effectively equivalent across the different conditions. The data from both samples, as-deposited and post-cleaning, are important because as-deposited is the condition subsequent layers are built on top of, while post-cleaning measurements serve as a more direct measure of substrate adhesion.

When analyzing the perpendicular profiles line roughness results, a decision was made to deliberately select defect-free areas to expand the usable sample size. Results where defects were avoided are presented here, whereas results where the full specimen surface including the defected

regions were analyzed are available in the Appendix. For example, the perpendicular roughness with defects, the results can be seen in Figure 19. Regarding the defect-free data, it can be seen again that the line roughness values are very similar across the different hatch spacings. From these results, it is also evident that the differences in morphology are of order the size of the deposited agglomerate, thus not providing a full picture of the effects on overall film morphology (Fig. 10).

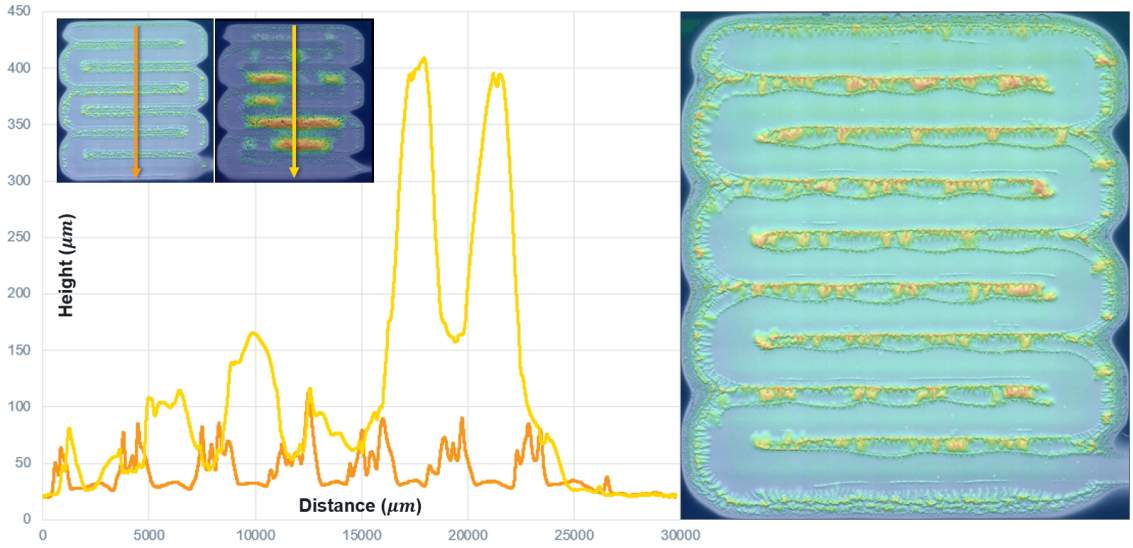

(a) Sample Line Measurements of Perpendicular Profiles (b) Standard Serpentine As-Deposited Sample

Figure 8: Digital microscope images of specimen. Perpendicular profiles demonstrate the variation in surface morphology due to defects, directly correlating to poor adhesion post-cleaning.

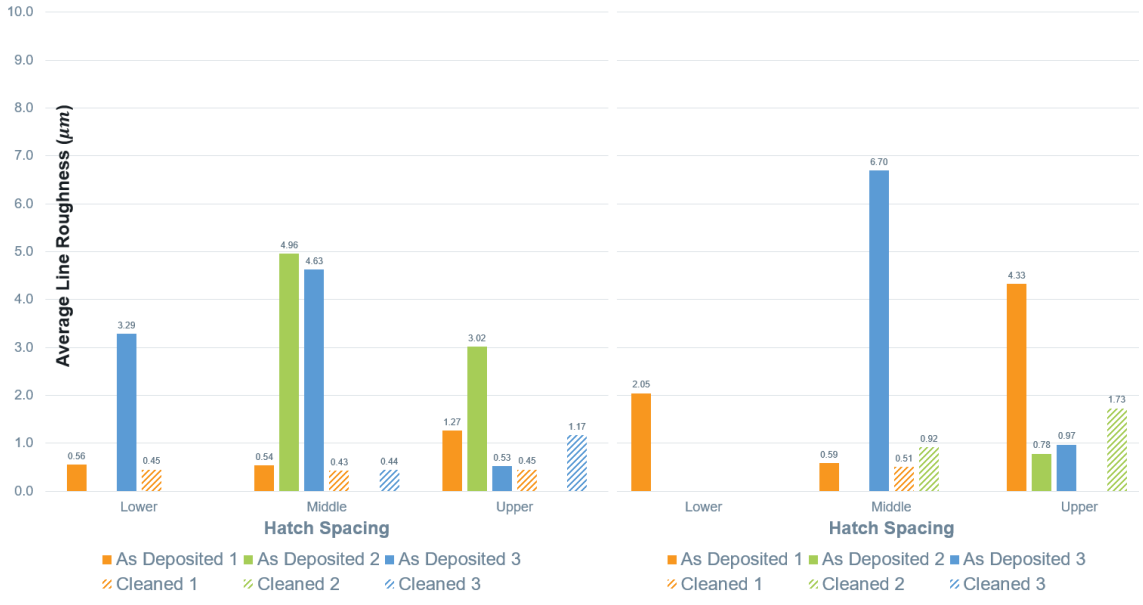

(a) Parallel Line Roughness for Serpentine (b) Parallel Line Roughness for Overlap

Figure 9: Summary of parallel profile line roughness results as-deposited and post-cleaning.

Therefore, to move beyond the influence of individual particles and instead capture the overall surface profile, it is necessary to examine the next structural scale in the morphology of the deposit. This requires shifting the focus from line roughness (R_a) to total line waviness (W_t), and correspondingly changing the scale of interest from 1–5 μm to 20–80 μm. By applying waviness filters, the contribution of individual particles is suppressed, allowing analysis of how they collectively shape the surface. In our study, we quantify this behavior using total waviness with cutoff parameters λ_s = none, λ_c = 800 μm, and λ_f = 2500 μm, thereby capturing the film morphology more clearly.

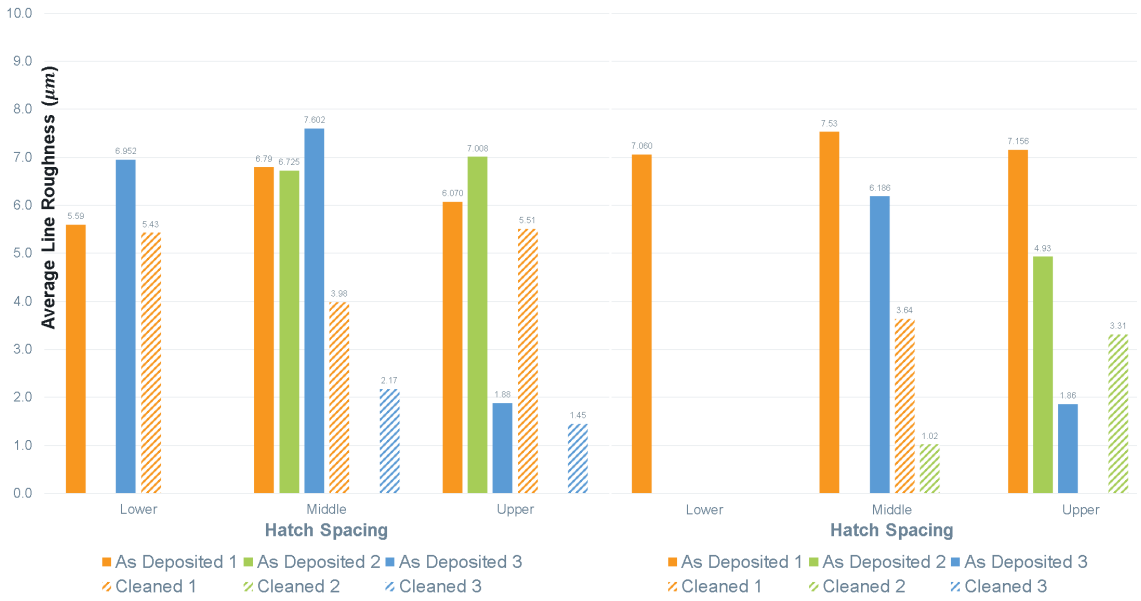

(a) Perpendicular Line Roughness for Serpentine (b) Perpendicular Line Roughness for Overlap

Figure 10: Summary of perpendicular profile line roughness results as-deposited and post-cleaning.

Parallel waviness measurements proved to be unsuitable as the surface was too smooth under the nozzle path. As can be seen in Figure 11, perpendicular waviness measurements in the defect-free regions showed similar performance between the lower and middle spaced spray patterns, while the upper spacing demonstrated slightly reduced waviness values. Since surface waviness measurements directly correlate with the flatness needed to build additional layers, this implies that the upper spacing configuration would yield the most favorable results for additive manufacturing applications.

Finally, an analysis that accounts only for the effect of hatch spacing and spray pattern across all samples is presented in Figure 12. These graphs reveal distinct trends for both as-deposited and cleaned conditions. As-deposited waviness decreased progressively with increasing hatch spacing. However, following cleaning, waviness values stabilized around 30 μm across all hatch distances. The comparison of spray pattern effects demonstrated that overlap patterns produced slightly lower values in the cleaned group compared to serpentine patterns. However, overlap patterns carried significantly higher delamination risks, with increased defect occurrence rates compared to serpentine configurations.

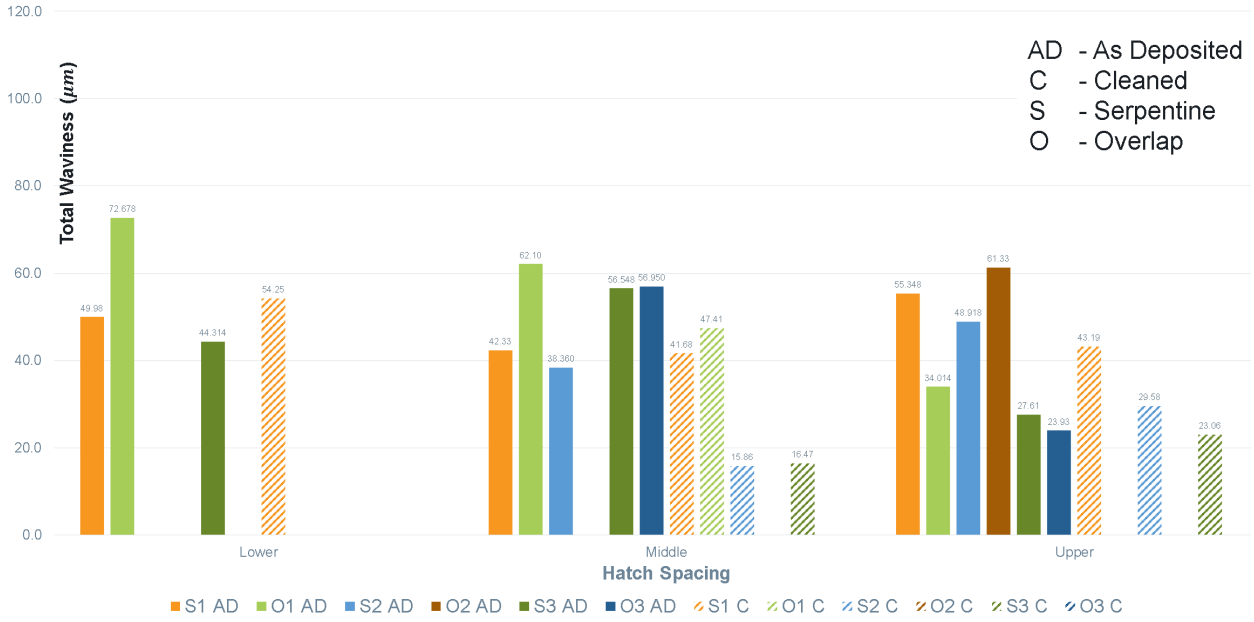

Figure 11: Summary of perpendicular profile waviness results as-deposited and post-cleaning.

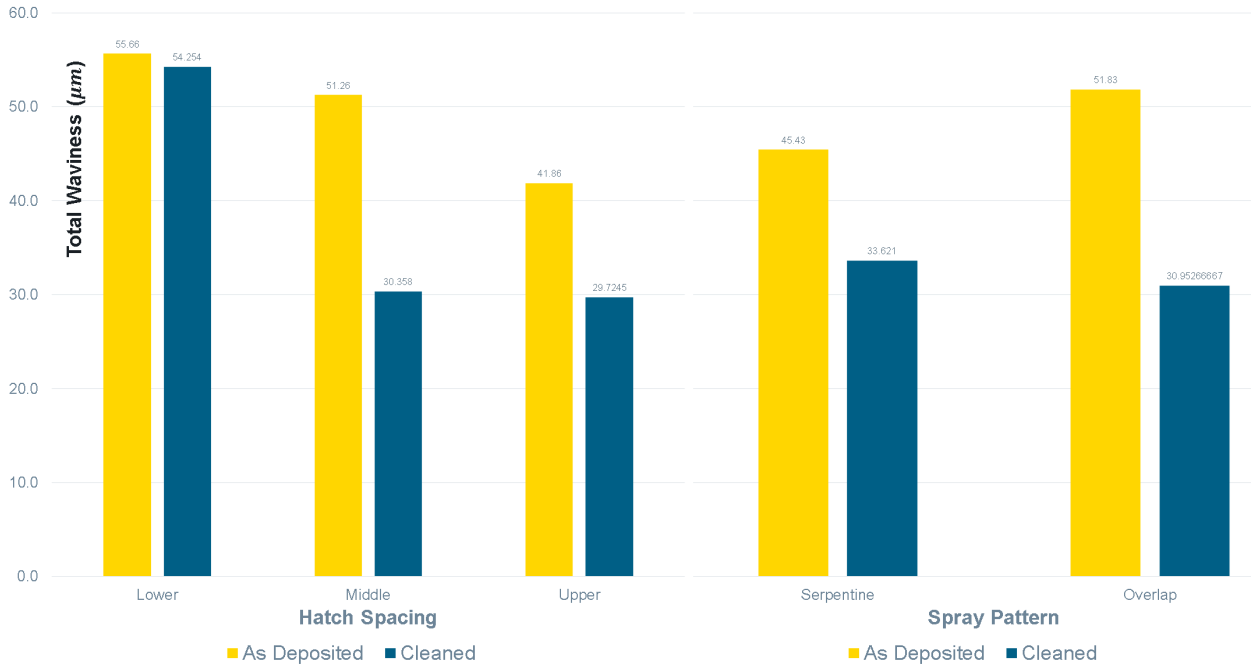

Figure 12: Hatch distance and spray pattern effects on total waviness.

For additive manufacturing applications where layer flatness is paramount, the results indicate that larger hatch spacings minimize surface waviness most effectively. This finding aligns with our observations that, for these very thick depositions, lower hatch spacings introduce excessive defect rates that compromise the reliability of the process. Thus, the data suggests that for such thick films, the optimal configuration for MCS additive manufacturing applications appears to be

larger hatch spacings with serpentine spray patterns, providing the best balance between surface flatness and process reliability while minimizing delamination risks.

6. Discussion

As the MCS machine used for these studies is a custom-built experimental apparatus rather than a commercial product, it is unsurprising that the deposition process exhibited noticeable run-to-run variability, particularly in terms of the deposition profile, both within a single run and across different runs, encompassing different time periods. Within a single run, as three varying serpentine patterns were deposited on a single silicon wafer, fluctuations in the width of the Gaussian deposition (6σ) were observed. This variability is believed to arise from multiple sources of uncertainties, including powder settling in the feeder and deagglomerator systems, nozzle degradation, and ambient humidity levels affecting powder flow. Other factors such as ambient temperature fluctuations and operator handling may also have contributed to this variability. While this variability invariably impacted the consistency of film morphology, general trends were still able to be observed, as discussed in Section 5. Further refinement in the design of the machine that address these variations would likely result in more consistent film morphologies.

Some films deposited in this study exhibited partial delamination, primarily due to two factors. The first relates to substrate choice: polished silicon wafers, have an extremely smooth surface, which hinders adhesion. Thus, while subsequent layers of deposited material bonded well to each other, the initial anchor layer (i.e., silver powder on the bare silicon) often detached, sometimes flaking off as a single sheet. Areas of failed adhesion left no visible marks or residue on the wafer after a light wipe, suggesting the absence of mechanical bonding. To mitigate this, future work could explore rougher substrates that provide more surface texture and compliance, thereby promoting stronger adhesion. The second factor concerns film thickness. Our films averaged 50–100 μm, far exceeding the 5–20 μm typically reported in the literature for thickness ranges produced by MCS. This design choice was intentional, as it allowed us to better study morphological characteristics. However, the increased thickness also heightened delamination risk, which was evident in several runs.

Future nozzle design optimization is also expected to enhance control over surface morphology. In our experiments, we used a commercial cold spray nozzle, which, given the agglomerate morphology, had a large throat diameter that resulted in a relatively flat deposition profile. A higher-resolution nozzle, by contrast, would be expected to yield a more peaked pseudo-Gaussian distribution of deposited material, enabling the fabrication of narrower features. This approach aligns directly with the concept of multi-resolution MCS that we plan to explore in future work. Within this paradigm, a larger nozzle can be employed for rapid bulk deposition, while a finer nozzle can subsequently refine the film, defining the final geometry and surface features with greater precision.

Finally, the current design of experiments, based on a traditional full factorial approach, is not the most efficient strategy for studying MCS. It could be improved to more rapidly assess the effects of process parameters, beyond hatch distance and spray pattern, on film surface morphology. One promising alternative is Bayesian experimental design (BED), which balances exploration and exploitation to guide parameter tuning in high-dimensional design spaces while significantly reducing the number of required experiments [20, 21]. A key challenge, however, is that BED depends

on an appropriate experimental model, which in this case would likely need to be physics-based. While such models have been successfully applied in cold spray (CS) [22], extending them to MCS remains difficult due to the limited understanding of its deposition physics. Another promising direction is transfer learning, where models developed for related spraying technologies [23] could provide a foundation for MCS, given their underlying similarities in manufacturing physics.

7. Conclusions

To conclude, we have studied the impact of hatch distance and spray pattern on the morphology of MCS films. Our design of experiments was grounded on a specific methodological framework in which we wanted to understand the benefits of overlapping serpentine patterns from pseudo-Gaussian deposition profiles produced by CS and MCS, and our interest in dual-nozzle systems which could leverage a higher-resolution nozzle to facilitate the creation of features with complex 3D geometries. To validate our model, we carried out physical experiments using ultrafine silver powder on silicon wafers on a custom-build MCS platform. Preliminary data suggests that serpentine patterns with larger hatch spacings are preferable due to a good balance of film flatness and low risk of delamination. Looking ahead, future work will focus on reducing run-to-run variability, assessing whether the observed trends extend to other substrates and powders, and developing more efficient experimental design strategies, such as BED- and ML-based approaches, to optimize process parameters for finer deposition geometry control.

Acknowledgement

The authors thank the Army Research Lab for supporting this work through grant number W911NF-24-2-0007. We would also like to thank Dr. Michael Gammage for guidance on the experimental methodology and Dr. Stephen Bierschenk for helpful discussions on the underlying physics of micro-cold spray.

References

[1] J. Akedo, "Aerosol deposition method for fabrication of nano crystal ceramic layer," in *Designing, Processing and Properties of Advanced Engineering Materials*, vol. 449 of *Materials Science Forum*, pp. 43–48, Trans Tech Publications Ltd, 4 2004.

[2] J. Akedo, "Aerosol deposition of ceramic thick films at room temperature: Densification mechanism of ceramic layers," *Journal of the American Ceramic Society*, vol. 89, no. 6, pp. 1834–1839, 2006.

[3] D. Hanft, J. Exner, M. Schubert, T. Stöcker, P. Fuierer, and R. Moos, "An overview of the aerosol deposition method: Process fundamentals and new trends in materials applications," *J. Ceram. Sci. Technol*, vol. 6, no. 3, pp. 147–182, 2015.

[4] A. Papyrin, V. Kosarev, S. Klinkov, A. Alkhimov, and V. M. Fomin, *Cold spray technology*. Elsevier, 2006.

[5] S. G. Bierschenk, M. F. Becker, and D. Kovar, "Gas and ceramic particle velocities for micro-cold spray," *Journal of Aerosol Science*, vol. 169, p. 106113, 2023.

[6] J. McCallister, M. Gammage, J. Keto, M. Becker, and D. Kovar, "Influence of agglomerate morphology on micro cold spray of ag nanopowders," *Journal of Aerosol Science*, vol. 151, p. 105648, 2021.

[7] J. Exner, P. Fuierer, and R. Moos, "Aerosol codeposition of ceramics: mixtures of bi2o3–tio2 and bi2o3–v2o5," *Journal of the American Ceramic Society*, vol. 98, no. 3, pp. 717–723, 2015.

[8] J. Akedo, "Room temperature impact consolidation (rtic) of fine ceramic powder by aerosol deposition method and applications to microdevices," *Journal of Thermal Spray Technology*, vol. 17, pp. 181–198, 2008.

[9] J. Henon, M. A. Piechowiak, O. Durand-Panteix, G. Etchegoyen, O. Masson, C. Dublanche-Tixier, P. Marchet, B. Lucas, and F. Rossignol, "Dense and highly textured coatings obtained by aerosol deposition method from ti3sic2 powder: Comparison to a dense material sintered by spark plasma sintering," *Journal of the European Ceramic Society*, vol. 35, no. 4, pp. 1179–1189, 2015.

[10] D. Vanerio, J. Kondas, M. Guagliano, and S. Bagherifard, "3d modelling of the deposit profile in cold spray additive manufacturing," *Journal of Manufacturing Processes*, vol. 67, pp. 521–534, 2021.

[11] R. Falco and S. Bagherifard, "Cold spray additive manufacturing: A review of shape control challenges and solutions," *Journal of Thermal Spray Technology*, pp. 1–19, 2025.

[12] Z. Cai, S. Deng, H. Liao, C. Zeng, and G. Montavon, "The effect of spray distance and scanning step on the coating thickness uniformity in cold spray process," *Journal of thermal spray technology*, vol. 23, pp. 354–362, 2014.

[13] H. Wu, X. Xie, M. Liu, C. Verdy, Y. Zhang, H. Liao, and S. Deng, "Stable layer-building strategy to enhance cold-spray-based additive manufacturing," *Additive Manufacturing*, vol. 35, p. 101356, 2020.

[14] D.-W. Lee, H.-J. Kim, Y.-H. Kim, Y.-H. Yun, and S.-M. Nam, "Growth process of α-al2o3 ceramic films on metal substrates fabricated at room temperature by aerosol deposition," *Journal of the American Ceramic Society*, vol. 94, no. 9, pp. 3131–3138, 2011.

[15] D.-W. Lee, H.-J. Kim, Y.-N. Kim, M.-S. Jeon, and S.-M. Nam, "Substrate hardness dependency on properties of al2o3 thick films grown by aerosol deposition," *Surface and Coatings Technology*, vol. 209, pp. 160–168, 2012.

[16] M. Lebedev and J. Akedo, "Patterning properties of pzt thick films made by aerosol deposition," *Ferroelectrics*, vol. 270, no. 1, pp. 117–122, 2002.

[17] R. F. Stone, M. Gammage, J. Wang, M. Cullinan, D. Kovar, and Z. Sha, "Multi-nozzle cooperation for micro-cold spray," 2024.

[18] J. McCallister, J. Keto, M. Becker, and D. Kovar, "Influence of normal velocity on microstructure and density of films produced by nanoparticle impact," *AIP Advances*, vol. 9, no. 3, 2019.

[19] D. J. Whitehouse, *Handbook of surface metrology*. Routledge, 2023.

[20] T. Rainforth, A. Foster, D. R. Ivanova, and F. Bickford Smith, "Modern bayesian experimental design," *Statistical Science*, vol. 39, no. 1, pp. 100–114, 2024.

[21] K. Chaloner and I. Verdinelli, "Bayesian experimental design: A review," *Statistical science*, pp. 273–304, 1995.

[22] H. Wu, X. Xie, M. Liu, C. Chen, H. Liao, Y. Zhang, and S. Deng, "A new approach to simulate coating thickness in cold spray," *Surface and Coatings Technology*, vol. 382, p. 125151, 2020.

[23] D. Ikeuchi, A. Vargas-Uscategui, X. Wu, and P. C. King, "Neural network modelling of track profile in cold spray additive manufacturing," *Materials*, vol. 12, no. 17, p. 2827, 2019.

Appendix

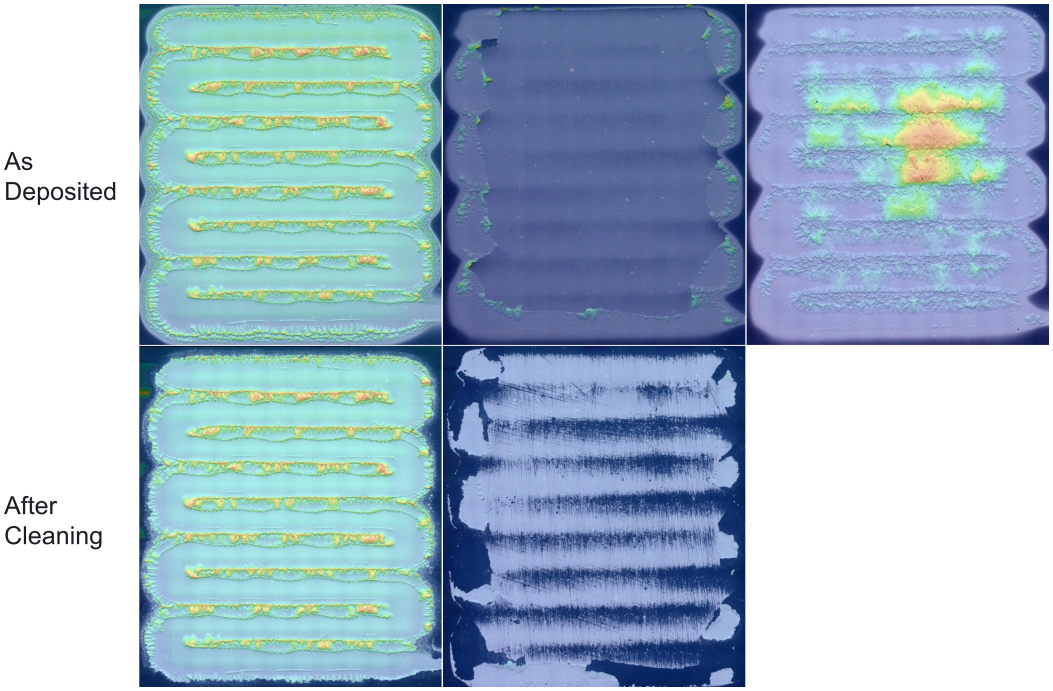

Figure 13: Serpentine Lower Spacing

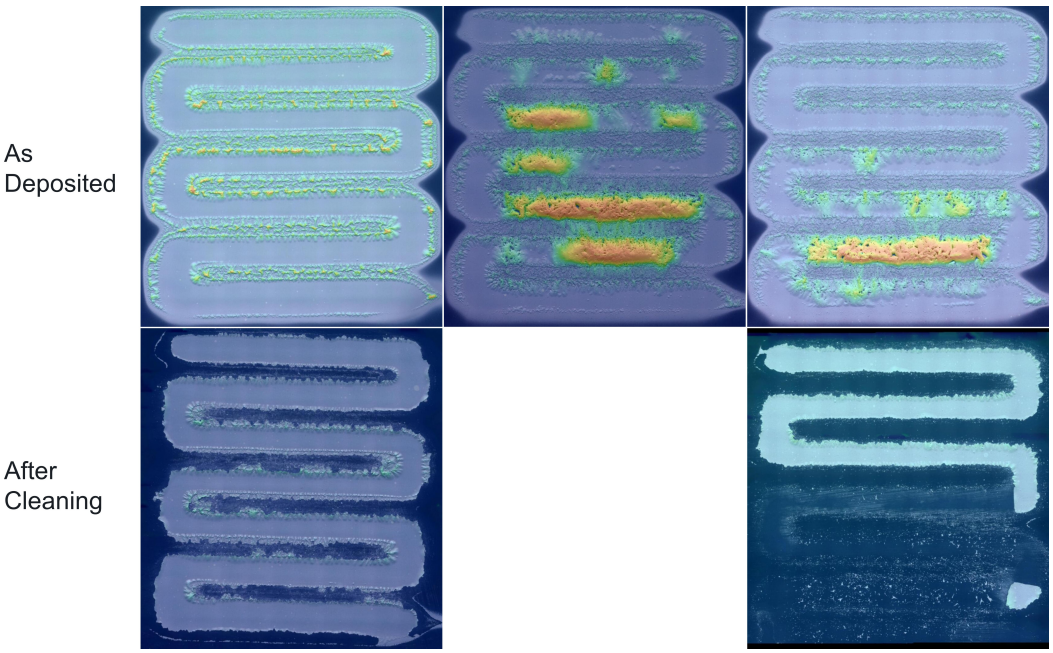

Figure 14: Serpentine Middle Spacing

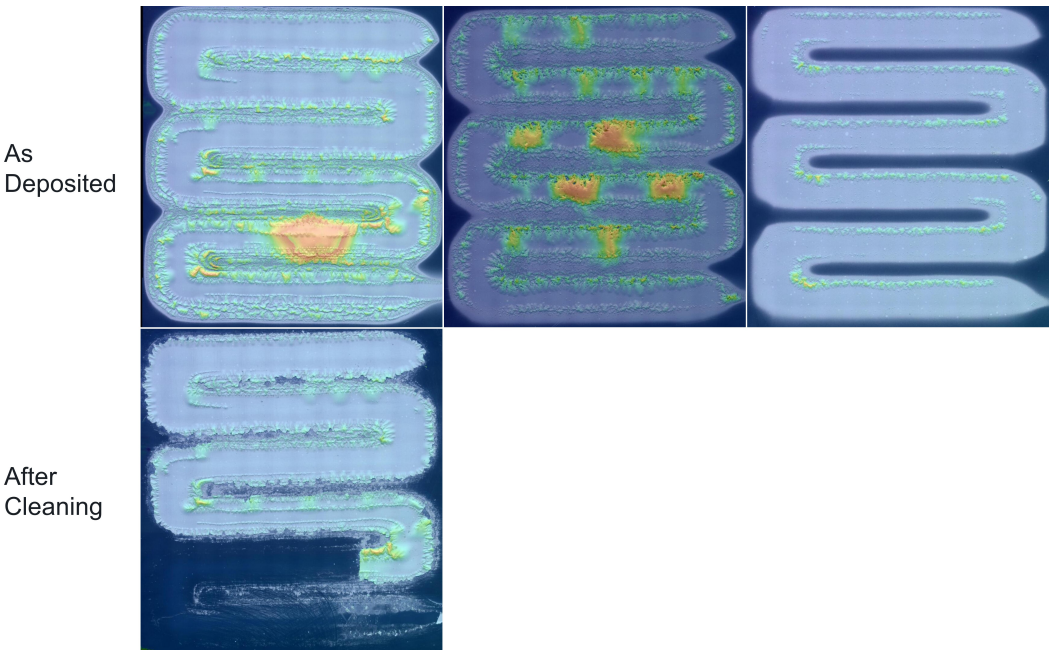

Figure 15: Serpentine Upper Spacing

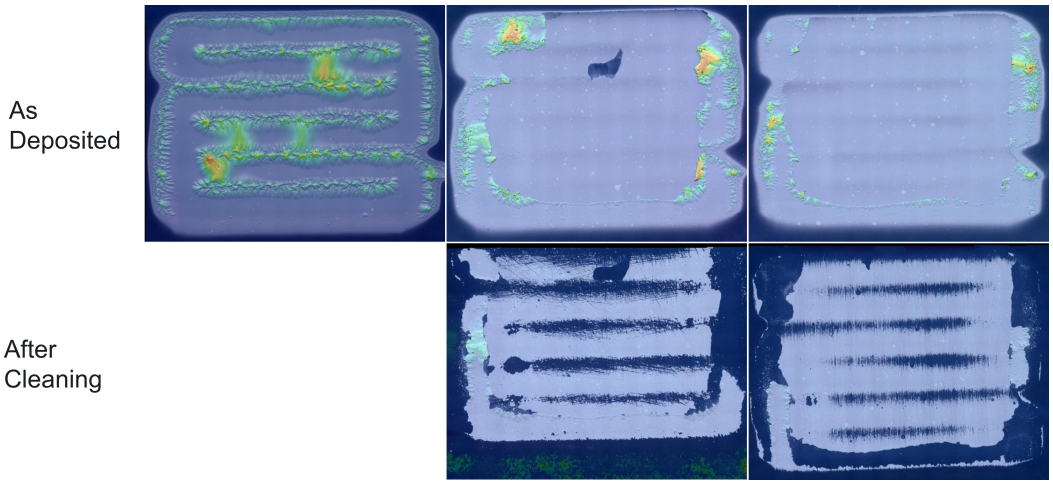

Figure 16: Overlap Lower Spacing

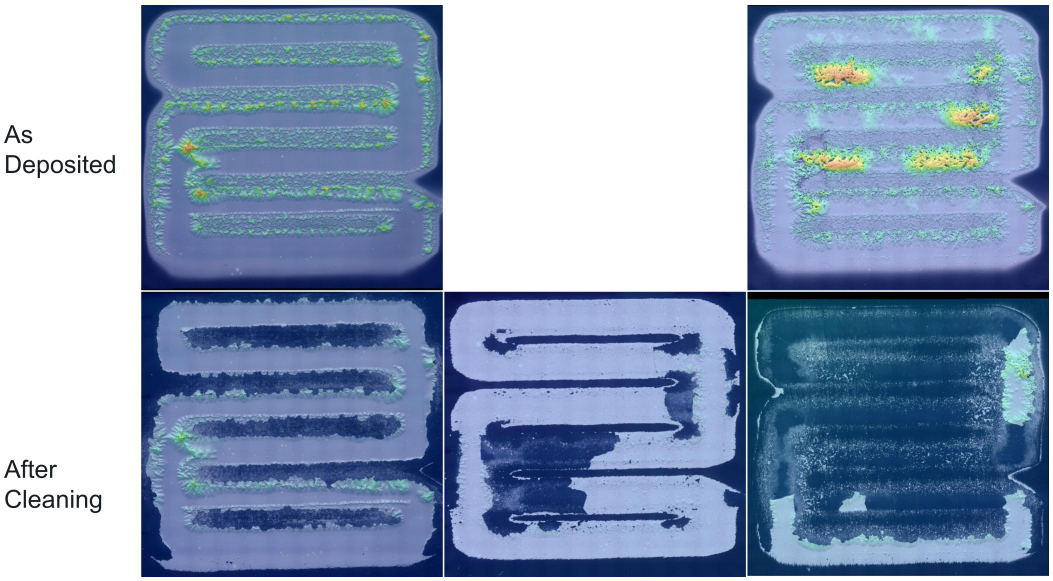

Figure 17: Overlap Middle Spacing

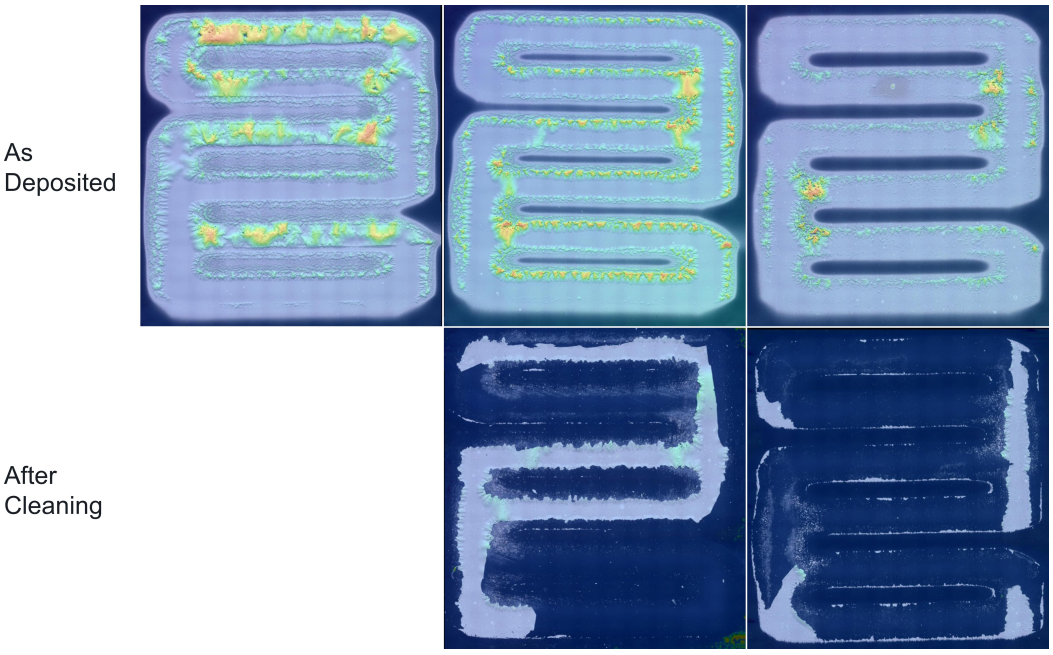

Figure 18: Overlap Upper Spacing

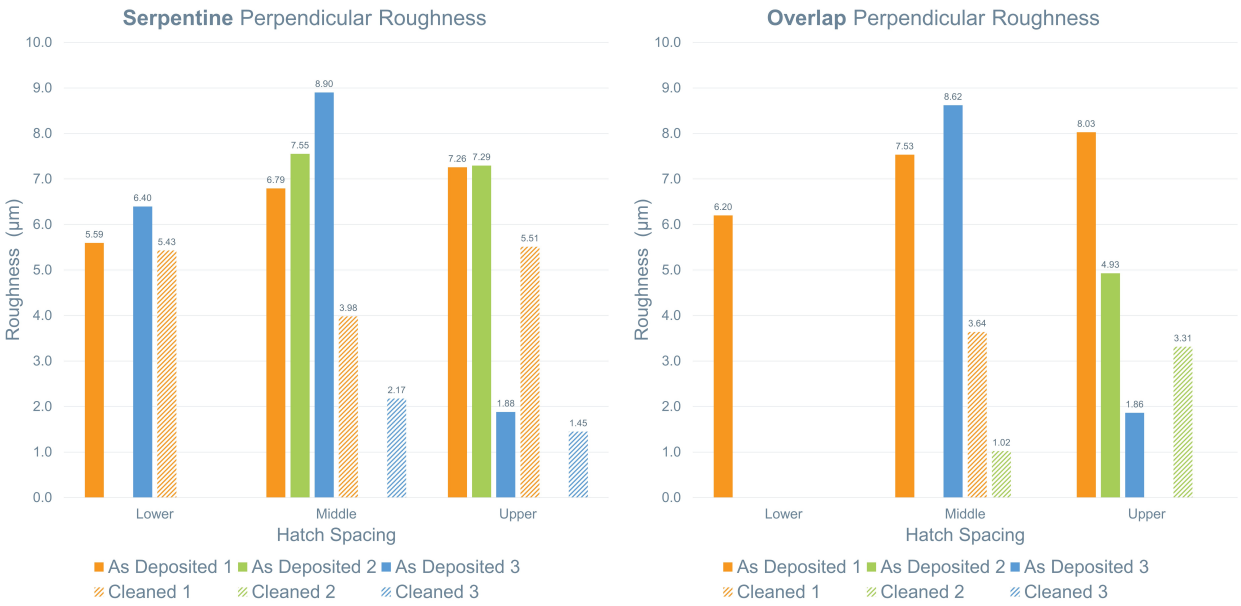

(a) Serpentine (b) Overlap

Figure 19: Perpendicular Roughness With Defects

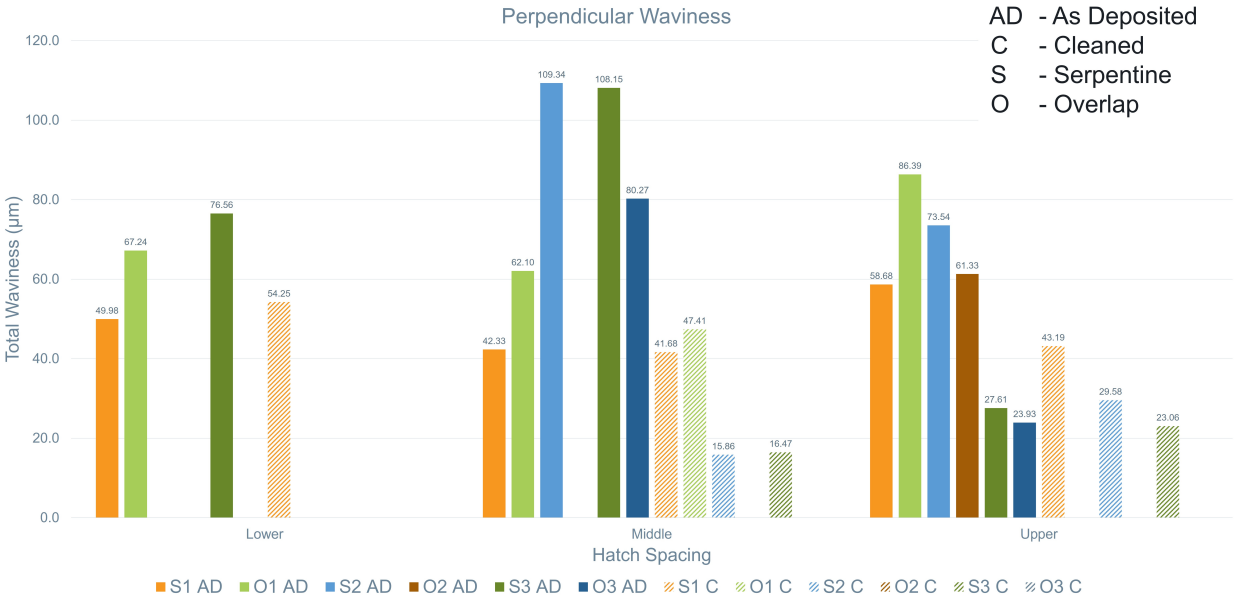

Figure 20: Perpendicular Waviness With Defects